Hexarhodium Clusters on Lanthana: Synthesis, Characterization, and Catalysis of Ethene Hydrogenation

Vinesh Bhirud, Jesse F. Goellner, Andrew M. Argo, and Bruce C. Gates*

Department of Chemical Engineering and Materials Science, University of California, Davis, California 95616

Received: January 27, 2004; In Final Form: April 21, 2004

Rhodium carbonyl clusters were prepared on the surface of La_2O_3 powder (calcined at 673 K) by a surface-mediated synthesis from La_2O_3-supported $Rh(CO)_2(acac)$ in the presence of CO at 1 atm and 373 K. The cluster preparation and subsequent decarbonylation by treatment in He were characterized by infrared (IR) and extended X-ray absorption fine structure (EXAFS) spectroscopies. Treatment in He at 573 K removed the carbonyl ligands, giving site-isolated La_2O_3-supported clusters that are well approximated as Rh_6 octahedra, being characterized by a first-shell Rh−Rh coordination number of 3.9 ± 0.4 at a distance of 2.64 ± 0.02 Å. The supported clusters were characterized by IR and EXAFS spectroscopies in the presence of ethene and H_2 reacting catalytically to give ethane. The EXAFS first-shell Rh−Rh coordination number was found to be about 4, consistent with the presence of Rh_6 octahedra, which are inferred to be the catalytically active species. IR spectra show that both hydrocarbons and hydride ligands were present on the working cluster catalyst, including π-bonded ethene and others, inferred to be ethyl, ethylidyne, and di-σ-bonded ethene. The concentration of hydride on Rh_6 increased during the initial induction period in a flow reactor as the catalytic activity increased almost proportionately; hydrides are inferred to be reactive intermediates. ^{1}H NMR spectroscopy showed that hydride remained on the clusters following catalysis. The results suggest that the hydrogenation of ethene on Rh_6/La_2O_3 proceeds by insertion of π-bonded ethene into a Rh−H bond to form ethyl, which is subsequently hydrogenated to give ethane. Rh_6/La_2O_3 is about 50 times more active for ethene hydrogenation catalysis than Rh_6/γ-Al_2O_3, and we suggest that the difference is related to the electron-donor properties of the supports.

Introduction

Site-isolated clusters are important as catalysts in both nature and industry. Examples include Cu_4 bound to histidine ligands in nitrous oxide reductase, which catalyzes denitrification.[1] Platinum clusters, consisting of about 5−12 atoms each, supported in LTL zeolite catalyze naphtha dehydrocyclization in the manufacture of benzene.[2]

The goal of understanding the influence of ligands and supports for such clusters on their catalytic properties has motivated the preparation of supported clusters that are uniform and susceptible to precise characterization.[3] A straightforward synthetic method involves the preparation of supported molecular metal carbonyl clusters as precursors, followed by removal of the carbonyl ligands without significant perturbation of the metal frame.[3]

Clusters with well-defined structures have been formed on various supports to provide a basis for understanding the effects of supports on cluster properties. For example, Rh_6 has been prepared on nearly neutral supports (e.g., TiO_2 [4] and zeolite NaY[5]) and on the weakly basic zeolite NaX,[6] but there are no reports of this cluster on the strongly basic support La_2O_3. Clusters such as Rh_6 have been found to be catalytically active for reactions including alkene hydrogenation; the size and composition of the cluster affect the activity.[7]

Adsorbates formed from alkenes and H_2 have been observed on surfaces of metal catalysts during reaction. For example, Backman and Masel[8] used electron energy loss spectroscopy to identify ethyl and ethylidyne ligands on Pt(111) during ethene hydrogenation. On the basis of measurements of the rates of hydrogenation of these species, the authors suggested that ethyl was a reactive intermediate and ethylidyne only a spectator. Cremer et al.[9] used sum frequency generation to characterize adsorbates on Pt(111) during ethene hydrogenation, observing ethyl, ethylidyne, di-σ-bonded ethene, and π-bonded ethene and concluding that ethene hydrogenation proceeded via hydrogenation of π-bonded ethene to give ethyl, which was hydrogenated to give ethane. Ohtani et al.[10] used IR reflection absorption spectroscopy to characterize adsorbates on Pt(111) during ethene hydrogenation catalysis, observing only di-σ-bonded ethene and ethylidyne and showing that the rate of hydrogenation did not depend on the coverage of the surface with either species. Argo and Gates[11,12] used infrared (IR) and extended X-ray absorption fine structure (EXAFS) spectroscopies during ethene hydrogenation on Rh_6 and on Ir_6 clusters supported on MgO, identifying the hydrocarbon ligands and concluding that these clusters were catalytically active species. In theoretical work, Neurock and van Santen[13] investigated this reaction on Pd(111), inferring a mechanism slightly different from those mentioned above, finding that, at low coverages of the surface with ethene, hydrogenation proceeds through a di-σ-bonded ethene intermediate, whereas at high coverages direct hydrogenation of π-bonded ethene is predominant.

In summary, although there is detailed information about alkene hydrogenation catalysis on metals in various forms, the reaction proceeds on surfaces populated by a variety of species, and ambiguities remain.[14] The complexity is compounded by the influence of adsorbates on the reactivities of coadsorbates[13] and the lack of clear evidence of the effects of supports.

10.1021/jp049626s CCC: $27.50
Published on Web 06/10/2004

In the present work, we report the formation of Rh_6 on La_2O_3 and the influence of this strongly basic support on the catalytic activity of Rh_6 for ethene hydrogenation. The precursor was chosen to be a hexarhodium carbonyl cluster ($[Rh_6(CO)_{15}]^{2-}$ or $[Rh_6C(CO)_{15}]^2$), because methods for preparing these precursors on supports have been developed.[4−6] IR and ^1H NMR spectroscopies were used to identify adsorbates formed on the clusters during catalysis, and EXAFS spectroscopy was used to characterize the structure of the clusters before and during catalysis. The results show that La_2O_3-supported Rh_6 clusters are extraordinarily active for ethene hydrogenation and maintain their structure under mild reaction conditions. The data also give evidence of the adsorbates present on the clusters during catalysis.

Experimental Methods

Materials and Sample Handling. Sample syntheses and transfers were performed in the absence of moisture and air in a Braun MB-150M glovebox (purged with N_2 recirculating through traps containing particles of Cu and of zeolite 4A for O_2 and moisture, respectively) and a double manifold Schlenk vacuum line. N_2, H_2, He, and ethene with purities of 99.999% (Matheson) flowed through similar traps to remove traces of O_2 and water. CO (CP grade) was further purified by passage through a trap containing activated γ-Al_2O_3 particles and zeolite 4A, to remove any traces of metal carbonyls from the high-pressure gas cylinder and water, respectively. Tetrahydrofuran (THF) and *n*-hexane were dried over sodium benzophenone ketyl and deoxygenated with flowing N_2 prior to use. Bis-(triphenylphosphoranylidene)ammonium chloride, [PPN]Cl (Aldrich), and dicarbonylacetylacetonato rhodium(I), $Rh(CO)_2(acac)$ (Strem, 99%), were used as received.

High-area La_2O_3 was obtained from Rhone-Poulenc and had a BET surface area of 74 m^2/g. Deionized water was added to the La_2O_3 to form a paste, which was dried overnight in air at 393 K. The solid was ground and calcined as O_2 flowed through a bed of the particles as the temperature was ramped linearly from room temperature to 673 K and held for 2 h. The O_2 treatment was immediately followed by evacuation of the sample for 14 h at 673 K. The resultant La_2O_3 was then cooled to room temperature under vacuum, isolated, and stored in a N_2-filled glovebox. Since the high-area La_2O_3 obtained from Rhone-Poulenc was used up and we could not get more of this material, we also synthesized La_2O_3 by base hydrolysis of $La(NO_3)_3 \cdot 6H_2O$ with NaOH at 353 K in the presence of acetic acid. The resultant solid was washed thoroughly with deionized water and subsequently calcined at 673 K for 4 h to give La_2O_3, which was found to have a BET surface area of 74 m^2/g.[15] This lanthana was used for the Rh_6/La_2O_3 sample used for in-situ EXAFS measurements during ethene hydrogenation.

$Rh(CO)_2(acac)$ was combined with the calcined La_2O_3 and placed in a Schlenk flask in a N_2-filled glovebox. Dried and deoxygenated *n*-hexane was then introduced by cannula into the Schlenk flask. The resultant slurry was stirred for 1 day, and the solvent was removed by evacuation (pressure $<10^{-3}$ Torr) for 1 day. The resultant sample, containing 1 wt % Rh, was stored in the glovebox and later treated in a once-through flow reactor with CO at 1 atm and 373 K for 1 day to form La_2O_3-supported rhodium cluster carbonyls by surface-mediated synthesis.[16] The samples were decarbonylated in a once-through flow system, either a glass reactor or an EXAFS cell, in flowing He at 1 atm and 573 K.[17]

Ethene Hydrogenation Catalysis in a Plug-Flow Reactor. Ethene hydrogenation catalysis was carried out in a nearly isothermal, once-through tubular flow reactor at atmospheric pressure and temperatures ranging from 273 to 300 K. In the glovebox, inert, nonporous α-Al_2O_3 particles were mixed with the catalyst particles in a 100:1 ratio by mass of α-Al_2O_3 to catalyst and loaded into the reactor. The catalyst bed was held in the middle of the reaction zone by glass wool plugs. The packed reactor was isolated, removed from the glovebox, and installed in the flow system so that the catalyst did not come into contact with air.

The total feed flow rate (He + H_2 + ethene) to the flow reactor was typically 100 mL (NTP) min^{-1}. The catalyst mass was typically 10−20 mg. In kinetics experiments carried out at 273 K, the partial pressures were varied in the range of 40−300 Torr for ethene and 50−400 Torr for H_2 to determine the dependence of the reaction rate on the partial pressure of each reactant independently.

An on-line gas chromatograph (Hewlett-Packard, HP-5890 Series II), equipped with a 30 m × 0.53 mm DB-624 (J&W Scientific) capillary column (with N_2 as the carrier gas; 2.5 mL min^{-1}) and a flame-ionization detector, was used to analyze the reaction products. Conversions of ethene to ethane were less than 5%, so the reactor operated in the differential mode.[1] The reaction rates were determined from differential conversions with an accuracy of about ±10%.[18]

IR Spectroscopy. Transmission spectra were recorded with a Bruker IFS-66v spectrometer with a spectral resolution of 4 cm^{-1}. Samples were self-supporting wafers of the catalyst that were loaded into the cell in the glovebox. Each sample was scanned 64 times and the data were averaged.

Extraction of Rhodium Carbonyls from La_2O_3. Surface-bound rhodium carbonyls were extracted from the La_2O_3 by contacting the solid in a Schlenk flask with a deoxygenated solution of THF or [PPN]Cl in THF. The mixtures were stirred for approximately 1 1/2 h and allowed to settle for at least 8 h. The supernatant solution was transferred by syringe into a solution IR cell, and the cell was sealed and the sample quickly scanned. The spectrum of THF was subtracted from each spectrum, which is the average of 64 scans.

IR Spectroscopy of Functioning Catalysts. An IR cell (In-situ Research and Instruments, Granger, IN) was used as a flow reactor allowing measurement of transmission spectra while treatment gases flowed over and through a catalyst wafer at temperatures ranging from 288 to 300 K and as the catalytic hydrogenation of ethene took place. Each sample was scanned 128−512 times at steady state, and the signal was averaged. Difference spectra were calculated by subtracting the spectrum of the sample in the presence of He from that of the sample in the treatment gas. When the absorption by the treatment gas was significant, the spectrum of the treatment gas was subtracted from that of the sample in the treatment gas.

^1H NMR Spectroscopy. Magic angle spinning NMR (MAS NMR) spectra were recorded with a Chemagnetics CMX-400 spectrometer at a frequency of 400.13 MHz. Samples in the glovebox were loaded into 7.5-mm (outside diameter) ZrO_2 rotors and sealed with double O-ring Teflon plugs. Spectra were obtained at 298 K at various spinning frequencies, typically 4.4 and 5.4 kHz, to distinguish centerbands from spinning sidebands. ^1H spectra were obtained with single-pulse excitation by use of a 90° pulse (8 μs) and 0.1−2-s relaxation delays that allowed for complete relaxation.

^{13}C NMR Spectroscopy. ^{13}C MAS NMR spectra were recorded with the same spectrometer at a frequency of 100.63 MHz. Samples in the glovebox were loaded into 7.5-mm (outside diameter) Teflon rotors and sealed with double O-ring

TABLE 1: Crystallographic Data Characterizing the Reference Compounds and Fourier Transform Ranges Used in the EXAFS Analysis

		crystallographic data			Fourier transform		
ref compd	shell	*N*	*R* (Å)	ref	Δk (Å^{-1})	Δr (Å)	n[a]
Rh foil	Rh−Rh 1st shell	12	2.687	26	2.86−19.60	1.60−3.12	3
Rh crystal[b]	Rh−Rh 2nd shell	6	3.796	26	1.00−20.00	0.00−8.00	0
Rh crystal[b]	Rh−Rh 3rd shell	24	4.649	26	1.00−20.00	0.00−8.00	0
Rh crystal[b]	Rh−Rh 4th shell	12	5.368	26	1.00−20.00	0.00−8.00	0
Rh_2O_3	Rh−O	6	2.050	30	2.67−15.69	0.00−2.10	2
$Ru_3(CO)_{12}$	Ru−C[c]	4	1.910	31	3.71−14.80	0.95−1.87	1
	Ru−O*[d]	4	3.050	31	3.75−14.80	1.90−3.11	2
$LaRhO_3$[b]	Rh−La	2	3.961	27	0.00−20.00	0.00−8.00	0

[a] A k^n weighting was used in the Fourier transformation of the data for purposes of extracting the reference phase and amplitude functions of the absorber−backscatterer pair. [b] This reference file was calculated using the FEFF 7.0 software. [c] Used as the reference phase shift and backscattering amplitude for the Rh−C shells. [d] Used as the reference phase shift and backscattering amplitude for the Rh−O* shells.

Teflon inserts. Samples were rotated at rates from 3.3 to 4.0 kHz at the magic angle (54.4° relative to the magnetic field).

EXAFS Spectroscopy. EXAFS spectra were collected at beamline X-11A of the National Synchrotron Light Source (NSLS) at Brookhaven National Laboratory, Upton, NY, and at beamline 2-3 of the Stanford Synchrotron Radiation Laboratory (SSRL) at the Stanford Linear Accelerator Center, Stanford, CA. The storage ring electron energy was 2.5 GeV at NSLS and 3 GeV at SSRL; the beam current ranged from 140 to 240 mA at NSLS and from 50 to 100 mA at SSRL.

In a N_2-filled glovebox at the synchrotron, each powder sample was pressed into a self-supporting wafer. The mass was chosen to give an X-ray absorbance of approximately 2.5 at the Rh K edge. The wafer was loaded into an EXAFS cell,[17] sealed under a positive N_2 pressure, and removed from the glovebox. The cell was then evacuated (10^{-5} Torr), and the sample was aligned in the X-ray beam and cooled to nearly liquid nitrogen temperature. EXAFS spectra were then collected in transmission mode. A Si(220) double crystal monochromator at SSRL and a Si(111) double crystal monochromator at BNL were detuned by 20−25% at the Rh K edge to suppress higher harmonics in the X-ray beam. After EXAFS spectra had been collected, the samples were removed from the beamline and further treated in the EXAFS cell for 2 h with flowing He at a temperature between 373 and 573 K. The cell was then cooled to room temperature, reevacuated to 10^{-5} Torr, and cooled to nearly liquid nitrogen temperature. The sample was then scanned again, as described above.

Because of the significant absorption near the Rh K edge of X-ray energy by La in the support, we performed the in-situ EXAFS experiments in fluorescence mode to obtain a better signal-to-noise ratio than was attainable in the transmission experiments used otherwise. A fluorescence EXAFS cell consisting of a variable-temperature stainless steel body (approximated as a plug-flow reactor) sealed with Mylar windows[19] was used to characterize the sample in the presence of flowing He and also during catalysis (in the presence of flowing He, H_2, and C_2H_4 at reaction temperature). The EXAFS cell face on the X-ray incidence side was modified to allow measurements in fluorescence mode at NSLS (with a 13-element germanium detector). The powder catalyst was held in the middle of the reaction zone by glass wool plugs. A gas chromatograph (GOW-MAC, Series 600), equipped with a 30 m × 0.53 mm Supel-Q plot column (with N_2 as the carrier gas flowing at 3.0 mL min^{-1}) and a flame-ionization detector, was installed at the beamline for analysis of the product gas to quantify the catalytic activity. In the glovebox, the powder sample (0.15−0.18 g) was loaded into the EXAFS cell/reactor, which was then sealed, isolated, removed from the glovebox, and installed in the flow system at the beamline so that the catalyst did not come into contact with air.

Analysis of X-ray Absorption Spectra

Analysis of the data was based on experimentally determined reference files prepared from EXAFS data representing materials of known structure. EXAFS data characterizing rhodium foil and Rh_2O_3 were used for the phase shifts and backscattering amplitudes of the first-shell Rh−Rh and Rh−$O_{support}$ interactions. $Ru_3(CO)_{12}$ (which has only terminal CO ligands) mixed with X-ray-transparent BN was used to obtain the phase shifts and backscattering amplitudes used in analyzing the Rh−C and Rh−O* interactions (O* is carbonyl oxygen). (The transferability of the phase shifts and backscattering amplitudes for neighboring atoms in the periodic table has been justified experimentally.[20])

Analysis of the EXAFS data was carried out with a difference file technique[21,22] using the software XDAP.[23] Iterative fitting was carried out until satisfactory agreement was attained between the calculated k^0-, k^1-, k^2-, and k^3-weighted data and the postulated model (k is the wavevector).[22,23]

It was necessary to use a reference that exhibited multiple scattering, such as $Ru_3(CO)_{12}$, because the near linearity of the Rh−C−O moieties of terminally bound CO makes the influence of multiple scattering in the Rh−O* shells significant. The second Rh−Rh shell and the Rh−La reference files were calculated by using the code FEFF 7.0[24,25] and structural parameters representing a rhodium crystal[26] and $LaRhO_3$,[27] respectively. Details of the preparation of the reference files are presented elsewhere.[28,29] Table 1 is a summary of the parameters used to construct the reference files from the EXAFS data.[30]

The quality of the data obtained in the fluorescence mode was significantly better than that of the data obtained in the transmission mode, but in all cases the number of parameters used in fitting the data to each model was always less than the number justified statistically according to the Nyquist theorem.[31] The fitting ranges in both momentum and real space were determined by the data quality.

Results

Synthesis of Rh_6 Clusters Supported on La_2O_3. *Synthesis of Site-Isolated Supported Rhodium Dicarbonyls.* The following section includes evidence that the sample formed by chemisorption of $Rh(CO)_2(acac)$ on La_2O_3 contained predominantly site-isolated rhodium dicarbonyl complexes bonded to the La_2O_3. The number of ν_{CO} peaks in the IR spectrum and their positions (2079 s, 2009 vs cm^{-1}; Figure 1) are consistent with reports of

TABLE 2: IR Spectroscopic Data in the CO Stretching Region of Supported and Unsupported Rhodium Carbonyls

sample	ν_{CO}, cm^{-1}	ref
$Rh(CO)_2(acac)$ adsorbed on La_2O_3 calcined at 673 K	2078 s, 2009 vs, 1992 sh	this work
$Rh(CO)_2(acac)$ adsorbed on La_2O_3 calcined at 673 K, followed by treatment in CO at 373 K for 1 day	2100 w-sh, 2085 sh, 2059 vs, 2017 sh, 1936 w, 1897 sh, 1830 w	this work
surface species extracted with THF from $Rh(CO)_2(acac)$ adsorbed on La_2O_3 calcined at 673 K, followed by treatment in CO at 373 K for 1 day	2080 m, 2031 vs, 2010 s-sh, 1876 s, 1845 w-sh, 1830 w-sh	this work
surface species extracted with [PPN]Cl in THF from $Rh(CO)_2(acac)$ adsorbed on La_2O_3 calcined at 673 K, followed by treatment in CO at 373 K for 1 day	2055 s, 1975 vs, 1828 vw-sh, 2112 vw, 2032 s, 1876 s, 1847 m	this work
$Rh(CO)_2(acac)$ adsorbed on zeolite NaX calcined at 573 K	2087 s, 2006 vs	6
$Rh(CO)_2(acac)$ adsorbed on zeolite NaX calcined at 573 K, followed by treatment in CO at 398 K for 12.5 h	2100 w, 2050 sh, 2015 s, 1995 sh, 1738 sh	6
Rh aggregates supported on γ-Al_2O_3	terminal, 2060−2040 (1 peak); bridging, 1850	33
$Rh_6(CO)_{16}$ in KBr	2073, 2026, 1800	this work
$Rh_6(CO)_{16}$ in THF	2075 vs, 2043 w, 1809 m	this work
$Rh_6(CO)_{16}$ in [PPN]Cl and THF	2091 w, 2056 vs, 2044 s-sh, 2019 m, 1976 w, 1830 w, 1795 m	this work
$[Rh_6(CO)_{15}]^{2-}$ in CH_3CN	2048 w, 1990 s, 1960 s, 1815 w br, 1760 s	32
$[Rh_6(CO)_{15}C]^{2-}$ in THF	2030 w, 1993, 1883, 1843, and 1831 s	34

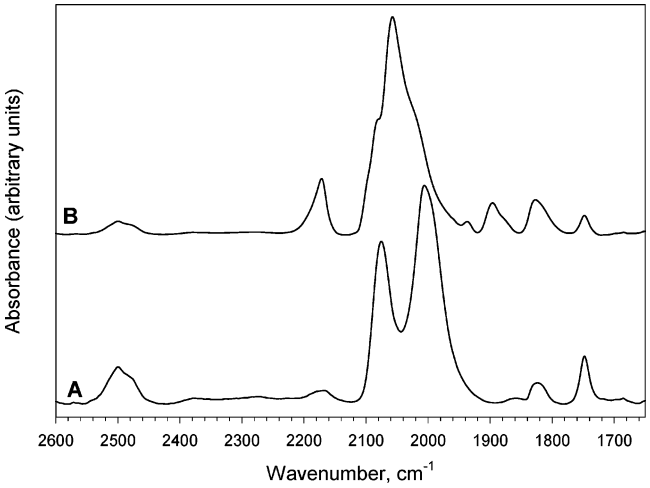

Figure 1. IR spectra in the carbonyl stretching region of rhodium carbonyls supported on La_2O_3 calcined at 673 K. (A) Species formed by chemisorption of $Rh(CO)_2(acac)$; (B) species formed by chemisorption of $Rh(CO)_2(acac)$ followed by treatment in CO at 373 K for 24 h.

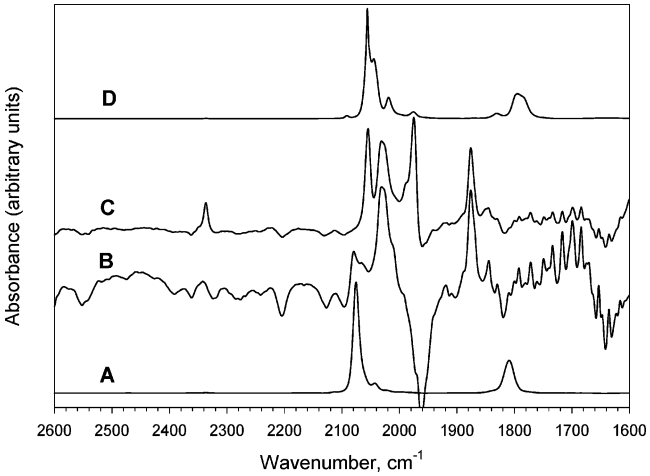

Figure 2. IR spectra in the ν_{CO} region of rhodium carbonyls. (A) $Rh_6(CO)_{16}$ in THF solution; (B) species extracted into THF from the surface of the sample formed by chemisorption of $Rh(CO)_2(acac)$ on La_2O_3 calcined at 673 K following treatment in CO at 373 K for 24 h; (C) species formed by chemisorption of $Rh(CO)_2(acac)$ on La_2O_3 calcined at 673 K following treatment in CO at 373 K for 24 h extracted into solution of [PPN]Cl in THF; (D) $Rh_6(CO)_{16}$ in a solution of [PPN]Cl in THF.

supported rhodium dicarbonyls (e.g., 2087 s, 2006 vs cm^{-1} for the complex on zeolite NaX calcined at 573 K[6]) (Table 2). The IR peaks characterizing $Rh(CO)_2$ on La_2O_3 are not excessively broad, nor do they include any shoulders which might imply that the $Rh(CO)_2(acac)$ adsorbed in multilayers or as crystallites; the signal-to-noise ratio is high (Figure 1).

Surface-Mediated Synthesis To Form Hexarhodium Carbonyl Clusters. Treatment of the sample formed by chemisorption of $Rh(CO)_2(acac)$ on La_2O_3 with CO at 373 K for 1 day converted the surface rhodium species predominantly into rhodium carbonyl clusters that are inferred to be $[Rh_6(CO)_{15}]^{2-}$ and/or $[Rh_6C(CO)_{15}]^{2-}$. The IR spectrum of the solid sample made by treating site-isolated La_2O_3-supported $Rh(CO)_2$ in CO at 373 K for 1 day (2100 w-sh, 2086 vs, 2032 m-sh, 2020 s, 1847 w-sh, 1828 m cm^{-1}; Figure 1) indicates terminal and bridging CO ligands and thus the presence of rhodium carbonyl clusters. The ν_{CO} bands of the supported rhodium carbonyl clusters formed by reductive carbonylation can be interpreted as shifted and broadened relative to the spectra of rhodium carbonyl clusters in solution (as expected for metal carbonyls interacting with a polarizing, nonuniform support such as La_2O_3). The spectra of the La_2O_3-supported rhodium carbonyl clusters are similar to that of $[Rh_6(CO)_{15}]^{2-}$ [32] in solution (Table 2)[33] and also to that of $[Rh_6C(CO)_{15}]^{2-}$ [34] and $Rh_6(CO)_{16}$[35] ($Rh_6(CO)_{16}$ is a neutral species that is not expected on a basic support). Thus, although the IR spectra point to hexarhodium carbonyls, they are not sufficient to identify the specific supported clusters.

The conversion of La_2O_3-supported $Rh(CO)_2(acac)$ into La_2O_3-supported rhodium carbonyl clusters is confirmed by the IR spectrum of the weakly bound species extracted from the La_2O_3 into THF. The spectrum of the extracted species (2080 m, 2031 vs, 2010 s-sh, 1876 s, 1845 w-sh, 1830 w cm^{-1}; Figure 2) includes bridging and terminal ν_{CO} bands, consistent with rhodium carbonyl clusters; the spectrum appears to be a superposition of the spectra of $[Rh_6C(CO)_{15}]^{2-}$ (2030 w, 1993, 1883, 1843, and 1831 s cm^{-1}) and $[Rh(CO)_2(acac)]$ (2081 s, 2010 vs cm^{-1}) in THF solution. When the surface species were extracted into THF solutions containing [PPN]Cl, the resultant spectrum (2055 s, 1974 vs, 2032 s, 1876 s, 1847 m, 1828 vw-sh cm^{-1}) was similar to a superposition of the spectra formed by dissolution of $Rh_6(CO)_{16}$ in a THF solution of [PPN]Cl, and $[Rh_6(CO)_{15}]^{2-}$ and $[Rh_6C(CO)_{15}]^{2-}$ dissolved in THF (Table 2). In summary, these spectra are too complex to allow identification of the extracted species, but they confirm the conversion of the La_2O_3-supported rhodium into clusters without determining whether they are neutral or charged or how many atoms they contain.

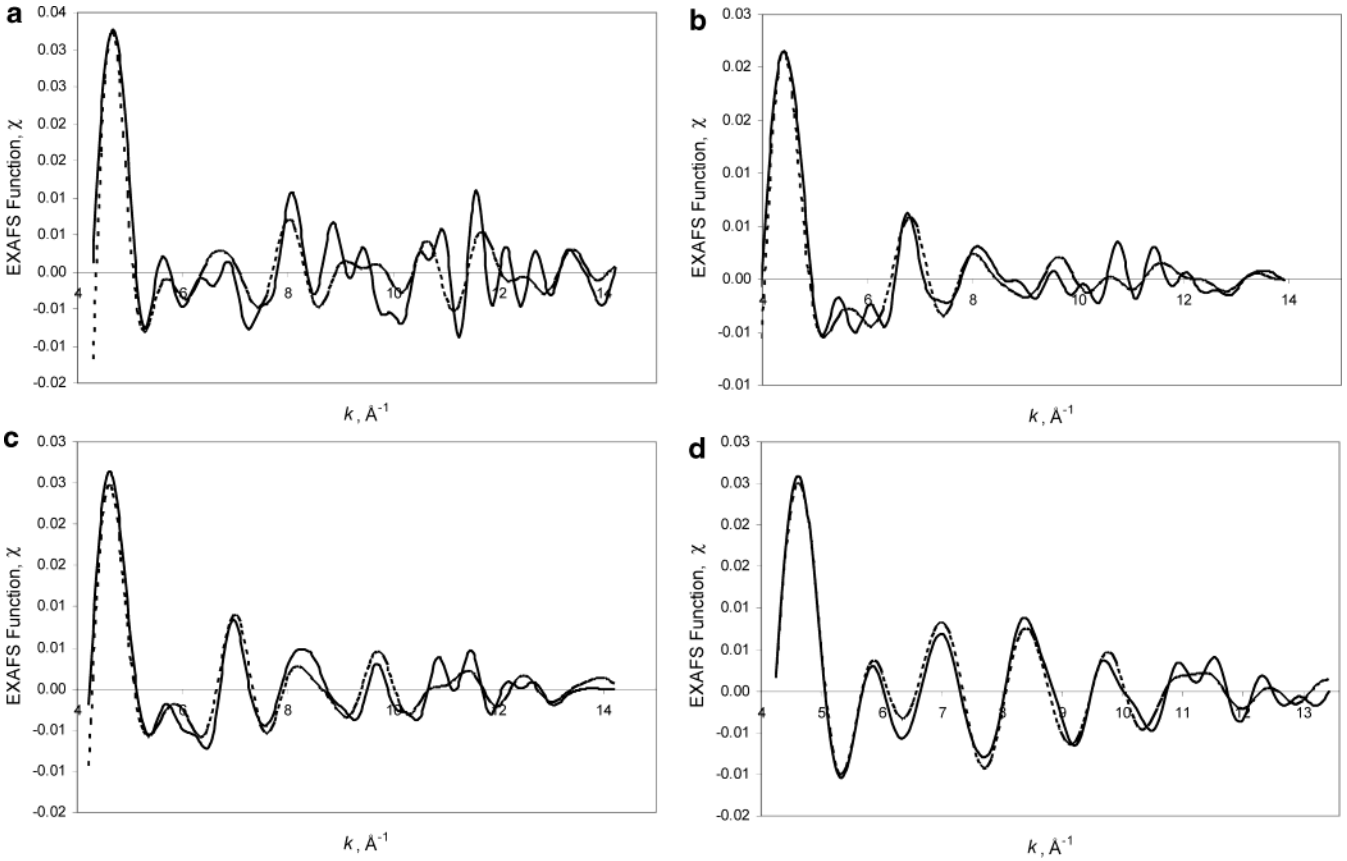

Figure 3. Results of EXAFS data analysis for La_2O_3-supported rhodium carbonyls and surface species formed by decarbonylation of rhodium carbonyls: EXAFS function, χ (solid lines), and calculated contributions (dotted lines) according to the reported structural parameters for (a) the species formed by chemisorption of $Rh(CO)_2(acac)$ on La_2O_3 calcined at 673 K and subsequent treatment in CO at 373 K for 24 h, (b) the sample from (a) following treatment in He at 373 K for 2 h, (c) the sample from (b) following treatment in He at 473 K for 2 h, and (d) the sample from (c) following treatment in He at 573 K for 2 h.

The EXAFS data confirm that La_2O_3-supported $Rh(CO)_2$ was converted into rhodium carbonyl clusters by treatment with CO at 373 K for 24 h (Figures 3 and 4). The Rh−Rh contributions in the EXAFS spectra consist of a first shell with a coordination number N of 4.3 ± 0.4 and a distance R of 2.76 ± 0.02 Å and a second shell with N = 1.1 ± 0.4 and R = 3.88 ± 0.02 Å (where the error bounds represent precisions and not accuracies; Table 3). These contributions are consistent, within the typical accuracy of such EXAFS data (N, ±10%; R, ±0.03 Å; $\Delta\sigma^2$, ±20%; ΔE_0, ±20%),[36] with the octahedral rhodium frame in $[Rh_6(CO)_{15}]^{2-}$ (and also in the neutral cluster $Rh_6(CO)_{16}$). The expected parameter values for these octahedral rhodium clusters from X-ray diffraction (XRD) data are the following: Rh−Rh, first shell: N = 4, R = 2.77 Å; Rh−Rh, second shell: N = 1, R = 3.92 Å.[37,38]

Because crystalline $[Rh_6C(CO)_{15}]^{2-}$ has a trigonal-biprismatic frame, as shown by XRD data,[39] the EXAFS spectra of this species would be expected to indicate two Rh−Rh shells, one characterized by a coordination number of 2 at a distance of 3.91 Å and the other (N = 3; $R \approx$ 2.80 Å) representing a superposition of two inequivalent Rh centers at distances that are difficult to distinguish. The EXAFS data (Table 3) are not consistent with the structure of $[Rh_6C(CO)_{15}]^{2-}$, but they do not rule out the possibility that a fraction of the supported species were $[Rh_6C(CO)_{15}]^{2-}$, because the Rh−Rh shells of this anion are characterized by distances similar to those expected for Rh_6 octahedra.

Although the quality of these transmission EXAFS data is not high and they do not determine the Rh−CO contributions more than qualitatively, they do indicate Rh−CO contributions consistent with the presence of both terminal and bridging CO ligands, as expected (on the basis of IR and XRD data) for $[Rh_6(CO)_{15}]^{2-}$ and/or $[Rh_6C(CO)_{15}]^{2-}$. The sample formed by carbonylation of La_2O_3-supported $Rh(CO)_2$ is characterized by $Rh-C_{terminal}$ (N = 2.8, R = 1.92 Å) and $Rh-C_{bridging}$ (N = 2.3, R = 2.13 Å) contributions, as expected for rhodium carbonyl clusters, but the nearly equal distances and similar phases of the two Rh−O* contributions expected for rhodium carbonyl clusters with both terminal and bridging CO ligands make it difficult to separate these contributions. Consequently, a single, broad Rh−O* contribution (N = 1.9, R = 2.88 Å), representing a superposition of $Rh-O^*_{terminal}$ and $Rh-O^*_{bridging}$, is used as an approximation to represent the La_2O_3-supported hexarhodium carbonyl clusters.

The representations of the cluster−support interface are imprecise because of the limited data quality and the general difficulty in determining metal−support interface structures by metal-edge EXAFS spectroscopy.[40] In our data analysis, the interface between the rhodium carbonyl clusters and the La_2O_3 support surface is characterized by two small Rh−La contributions (N = 0.5, R = 2.60 Å and N = 1.0, R = 3.45 Å) indicative of the proximity of the clusters to La atoms in a subsurface support layer. The contribution at R = 3.45 Å has not been determined with confidence; the uncertainty is associated with the difficulty of separating and distinguishing Rh−La and/or $Rh-O_{long}$ contributions; we do not rule out the latter.

The La_2O_3-supported rhodium carbonyl clusters are characterized by resonances at 168, 200, and 246 ppm in the ^{13}C MAS NMR spectra. All other resonances in the spectra are either spinning sidebands or representative of the rotor. The resonance

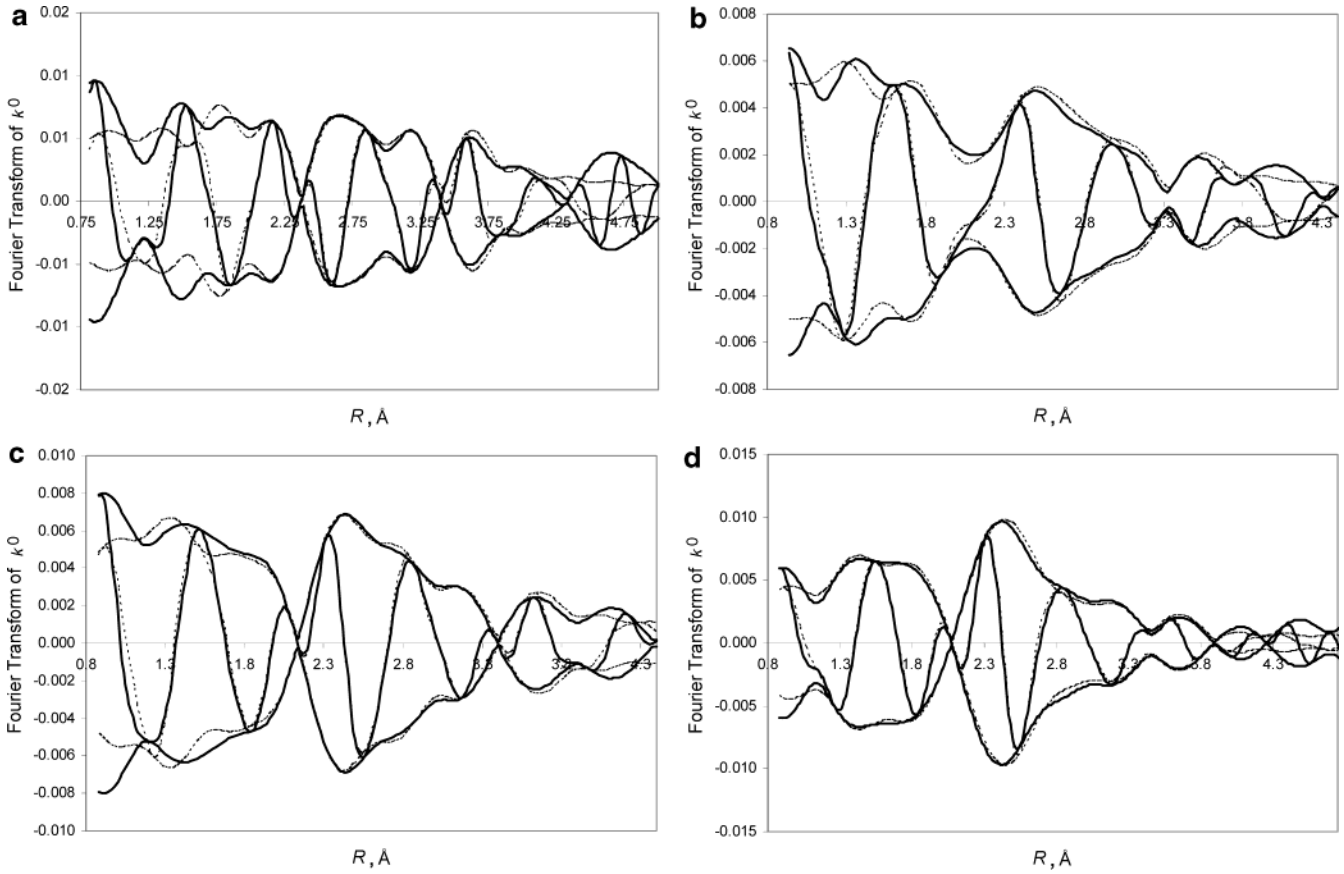

Figure 4. Results of EXAFS data analysis for La_2O_3-supported rhodium carbonyls and surface species formed by decarbonylation of rhodium carbonyls: imaginary part and magnitude of the k^0-weighted Fourier transform of raw data (solid lines) and calculated contributions (dashed lines) according to the reported structural parameters for (a) the species formed by chemisorption of $Rh(CO)_2(acac)$ on La_2O_3 calcined at 673 K and subsequent treatment in CO at 373 K for 24 h ($\Delta k = 4.29-14.21$ Å^{-1}), (b) the sample from (a) following treatment in He at 373 K for 2 h ($\Delta k = 4.00-14.51$ Å^{-1}), (c) the sample from (b) following treatment in CO at 473 K for 24 h followed by treatment in He at 473 K for 2 h ($\Delta k = 4.25-14.18$ Å^{-1}), and (d) the sample from (c) following treatment in He at 573 K for 2 h ($\Delta k = 4.24-13.42$ Å^{-1}).

TABLE 3: EXAFS Parameters Characterizing Rhodium Clusters Supported on La_2O_3 Powders Resulting from Chemisorption of $Rh(CO)_2(acac)$ on La_2O_3 Calcined at 673 K and Reductive Carbonylation in CO at 373 K for 1 day[a]

	no treatment				He, 373 K, 2 h				He, 473 K, 2 h				He, 573 K, 2 h			
backscatterer	N	R (Å)	$\Delta\sigma^2 \times 10^3$ (Å^2)	ΔE_o (eV)	N	R (Å)	$\Delta\sigma^2 \times 10^3$ (Å^2)	ΔE_o (eV)	N	R (Å)	$\Delta\sigma^2 \times 10^3$ (Å^2)	ΔE_o (eV)	N	R (Å)	$\Delta\sigma^2 \times 10^3$ (Å^2)	ΔE_o (eV)
rhodium																
1st shell	4.3	2.76	4.91	−5.66	3.9	2.70	12.9	2.21	3.7	2.62	3.62	4.77	3.9	2.64	4.08	2.24
2nd shell	1.1	3.88	0.09	2.58	0.7	3.85	2.88	18.2	1.1	3.87	2.49	9.26	0.6	3.62	3.41	2.09
CO ligands																
$C_{terminal}$	2.8	1.92	2.69	−11.70	1.7	1.86	−0.36	13.4	1.4	1.92	−1.59	−0.11				
$C_{bridging}$	2.3	2.13	−3.63	−13.07	2.1	2.08	−0.21	7.64	0.5	2.10	−6.49	−12.7	0.7	2.13	−0.89	6.3
O*	1.9	2.88	0.50	3.04					1.8	2.83	0.56	6.1				
support contributions																
O_{short}													1.1	2.00	−3.08	−8.27
La 1st shell	0.5	2.60	8.79	10.74					0.5	2.94	3.46	4.44	1.2	2.71	10.2	6.51
La 2nd shell	1.0	3.45	4.02	17.01	0.6	3.46	10.00	18.1	0.3	3.50	7.53	8.33	0.5	4.04	1.29	9.79

[a] Treatments under the conditions shown were for 2 h.

at 168 ppm indicates carbon of terminally bound CO ligands (Figure 5). The other two resonances can be interpreted as indicating the carbon of two inequivalent bridging CO ligands, consistent with the identification of the supported clusters as $[Rh_6(CO)_{15}]^{2-}$. However, the latter two resonances could alternatively be interpreted as arising from the carbon atom of bridging CO ligands and the carbido carbon of $[Rh_6C(CO)_{15}]^{2-}$, respectively (the carbido carbon of $[Rh_6C(CO)_{15}]^{2-}$ in solution is characterized by a resonance at 264.7 ppm).[41] Hence, although the ^{13}C MAS NMR data are consistent with surface-bound hexarhodium carbonyl clusters, they do not provide a definitive identification of these clusters.

In summary, the IR, EXAFS, and NMR data indicate that rhodium carbonyl clusters with an octahedral hexarhodium frame were formed by the carbonylation of La_2O_3-supported $Rh(CO)_2$; the synthesis must have been a reductive carbonylation. Although the spectroscopic data do not specifically identify the rhodium carbonyl cluster(s), they narrow the possibilities to hexarhodium carbonyls, $[Rh_6(CO)_{15}]^{2-}$ and $[Rh_6C(CO)_{15}]^{2-}$ (and/or possibly $Rh_6(CO)_{16}$, which is not expected on a strongly basic support such as La_2O_3).

Decarbonylation of Hexarhodium Carbonyl Clusters To Form Rh_6. The IR spectra of the samples formed following treatment in He at 573 K for 2 h of the La_2O_3-supported

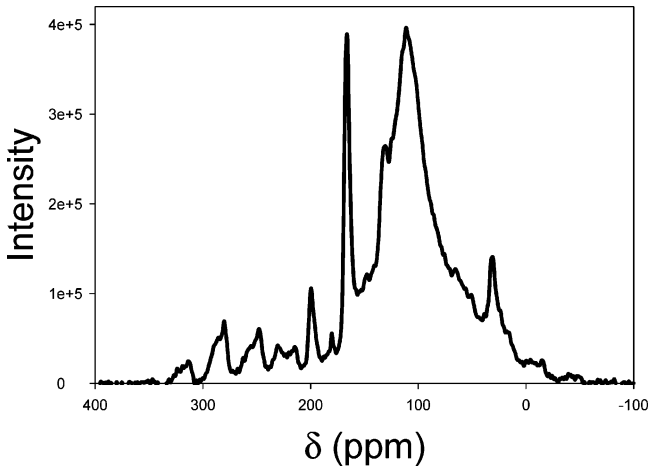

Figure 5. ^{13}C MAS NMR spectra of the sample formed by treating La_2O_3-supported $Rh(CO)_2$ with CO at 373 K for 1 day.

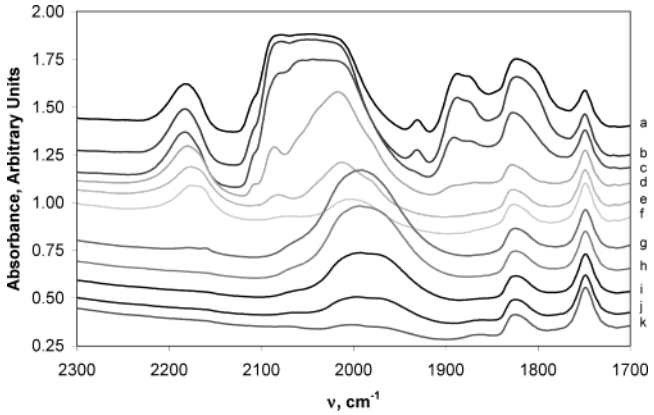

Figure 6. IR spectra of La_2O_3-supported hexarhodium clusters (formed from hexarhodium carbonyl clusters) measured in the presence of flowing He as the sample was heated from 298 to 573 K (a−g).

hexarhodium carbonyl clusters did not include CO stretching peaks (Figure 6), indicating that the decarbonylation was complete. The EXAFS results tracking the changes in these La_2O_3-supported clusters as the carbonyl ligands were removed are summarized in Table 3. These data show that the Rh_6 frame was essentially maintained during and after decarbonylation, as follows: After treatment of the La_2O_3-supported rhodium carbonyl clusters in He at 373 and 473 K, the samples were characterized by the two Rh−Rh shells (first shell: $N \approx 4$, $R \approx 2.7$ Å; second shell: $N \approx 1$, $R \approx 3.9$ Å) expected for a Rh_6 octahedron (Table 3). The sample after treatment in He at 573 K is represented by a Rh−Rh first-shell contribution ($N = 3.9$, $R = 2.64$ Å) and a Rh−Rh second-shell contribution ($N = 0.6$, $R = 3.62$ Å) consistent with a majority of the surface species having an octahedral Rh_6 frame.

The Rh−CO contributions diminished after treatment of the sample in He at 373 K and diminished further after treatment at 473 K (Table 3). The Rh−CO contributions were no longer present in the spectrum of the sample after treatment in He at 573 K; however, a small contribution tentatively attributed to Rh−C ($N = 0.7$, $R = 2.13$ Å) was observed. This contribution possibly represents some ill-defined and difficult-to-characterize carbon-containing ligands on the metal and originating from the carbonyl ligands. The possible nature of such presumed carbon-containing ligands is discussed elsewhere.[42]

Thus, the catalyst investigated in this work (formed by reductive carbonylation of La_2O_3-supported $Rh(CO)_2$ and subsequent decarbonylation in He at 573 K) is characterized as

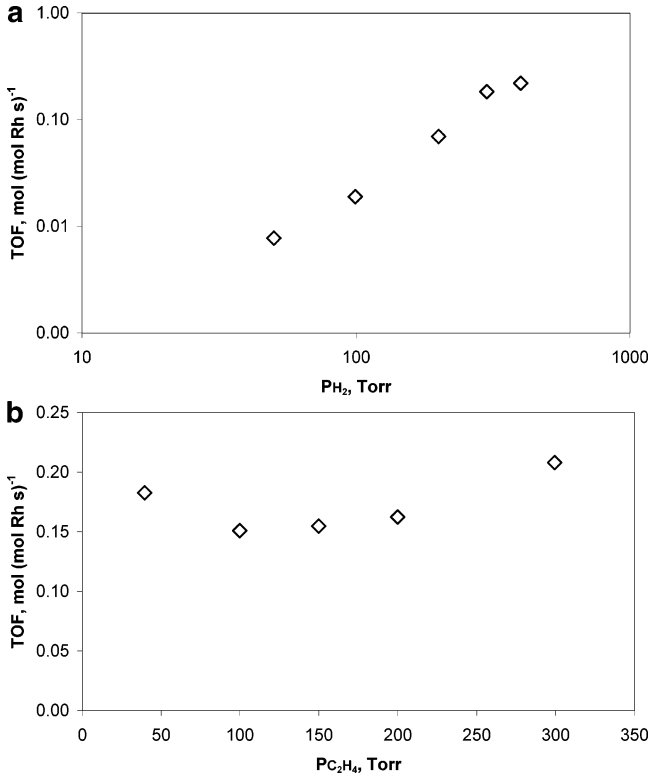

Figure 7. Ethene hydrogenation catalysis: dependence of reaction rate on (a) H_2 and (b) C_2H_4 partial pressures.

La_2O_3-supported Rh_6 clusters, with some ill-defined ligands such as carbon associated with them. It is unclear whether the carbon-containing species are bonded to the cluster frame or are present as carbido carbon atoms in the cluster interior.

Ethene Hydrogenation Catalyzed by Rh_6/La_2O_3. Rh_6/La_2O_3 was found to be catalytically active for ethene hydrogenation at 294 K. The catalytic activities (reported as turnover frequencies) were obtained from differential conversions calculated by assuming that all the Rh atoms were available for catalysis. There was no measurable conversion of ethene and H_2 in the absence of the catalyst (or in the presence of just the support) under the conditions of the experiments. Ethene hydrogenation catalyzed by Rh_6/La_2O_3 at 298 K and 760 Torr under conditions of continuous steady-state flow of reactant gases (348 Torr of H_2, 75 Torr of C_2H_4, and 337 Torr of He) was characterized by an induction period of about 4 h, during which the rate of ethene hydrogenation doubled as the catalyst reached steady state (time zero corresponds to the time at which He flow was replaced by reactant gas flow); it is possible that carbon on the clusters was removed during this period.

Data characterizing steady-state ethene hydrogenation following the induction period in catalysis by Rh_6/La_2O_3 at 273 K show that the reaction order in H_2 was 1.7 (Figure 7a). The reaction order in ethene was negative (−0.2) when the ethene partial pressure, $P_{C_2H_4}$, was <100 Torr and barely positive when the value of $P_{C_2H_4}$ was >100 Torr (Figure 7b). This dependence of the rate on ethene partial pressure is similar to that observed for conventional catalysts with extended metal surfaces.[13,43]

IR spectra of Rh_6/La_2O_3 recorded during isothermal ethene hydrogenation catalysis with continuous steady-state flow of reactants were collected at several times during the induction period to provide a basis for understanding the change in catalytic activity.

After gas-phase and support contributions had been subtracted from the spectra of Rh_6/La_2O_3 working as a catalyst for ethene

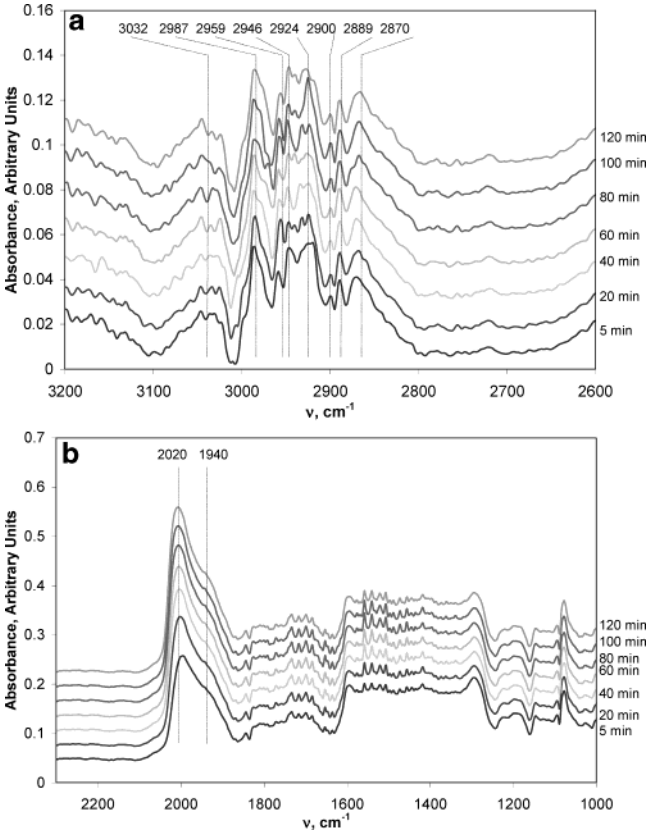

Figure 8. (a, top; b, bottom) IR spectra of adsorbates observed on Rh_6/La_2O_3 during the induction period for ethene hydrogenation catalysis at 298 K and 760 Torr (348 Torr of H_2 and 75 Torr of C_2H_4, balance He).

TABLE 4: IR Absorption Modes of Adsorbates on La_2O_3-Supported Rh_6 during Ethene Hydrogenation[a] and Vibrational Spectra of Reference Materials

material	adsorbate/compound	modes, cm^{-1}	ref
Rh(111)[a]	π-bonded ethene	3060, 3000	44
Rh(100)[a]	π-bonded ethene	3015, 2905	44
Rh_6/La_2O_3[b]	π-bonded ethene	3032	this work
Rh/Al_2O_3[c]	ethylidyne	2944, 2886	46
Rh(111)[a]	ethylidyne	2920, 2880	48
Rh_6/La_2O_3[b]	ethylidyne	2946, 2889	this work
Pt(111)[a]	di-σ-bonded ethene	3000, 2920	49,50
Fe(100)[a]	di-σ-bonded ethene	2985	51
Rh_6/La_2O_3[b]	di-σ-bonded ethene	2987, 2900	this work
CH_3CH_2Cl	CH_3CH_2Cl	2967, 2947, 2881	44
Rh(111)[a]	ethyl	2945	47
Rh_6/La_2O_3[b]	ethyl	2979/2959, 2924, 2870	this work

[a] Ultrahigh vacuum conditions. [b] Conditions for ethene hydrogenation in a flow reactor: 298 K, 348 Torr of H_2, 75 Torr of C_2H_4, 337 Torr of He, and total gas flow rate of 100 mL min^{-1}. [c] Vacuum.

hydrogenation, IR features corresponding to adsorbed hydrocarbons (adsorbates) were apparent (Figure 8a), indicated by features in the C−H stretching frequency range (2800−3200 cm^{-1}). The spectra are consistent with the superposition of the spectra of several adsorbates. Assignments of spectral features to individual adsorbates were made by comparing the vibrational frequencies with those of known ligands in reference compounds[44] and on rhodium,[45−48] platinum,[49,50] and iron surfaces[51] (Table 4). Data referred to elsewhere[10] for other supported metal cluster catalysts under conditions that lead to the predominance of individual hydrocarbon adsorbates provide a basis for identification of the individual adsorbates on the clusters during catalysis.

TABLE 5: Summary of IR Spectra: ν_{M-H} Stretching Frequencies Characterizing Metal Hydrides

sample	terminal metal hydride stretching frequencies, cm^{-1}	ref
hydride on Pt/Al_2O_3	2120, 2065	52
hydride on Pt/SiO_2	2130	53
$[RhH(NH_3)_5][SO_4]$	2079	54
$[RhH(NH_3)(en)_2][ClO_4]_2$ [a]	2025	55
hydride on Rh_6/La_2O_3	2020, 1940[b]	this work

[a] en = ethenediamine. [b] The large difference between the stretching frequencies of hydrides on Rh_6/La_2O_3 and of hydrides on Pt/Al_2O_3 is attributed to the change in metal and to La_2O_3 support effects.

The modes at 2946 and 2889 cm^{-1} are assigned to cluster-bound ethylidyne, because they occur at frequencies nearly identical to those of ethylidyne on rhodium particles supported on Al_2O_3 (2944 and 2886 cm^{-1}).[45] The modes at 2987 and 2900 cm^{-1} are assigned to di-σ-bonded ethene, because they occur at frequencies similar to those representing di-σ-bonded ethene on Pt(111) (3000 and 2920 cm^{-1}).[49] The mode at 3032 cm^{-1} is assigned to π-bonded ethene on Rh_6, because it occurs at a frequency similar to those of the vibrational modes of π-bonded ethene on Rh(111) (3060 and 3000 cm^{-1}). This mode is broad and weak, and thus it is not surprising that asymmetric and symmetric C−H stretches were not distinguishable. The remaining modes at 2959, 2924, and 2870 cm^{-1} are assigned to ethyl, because they occur at frequencies similar to those of ethyl chloride (2967, 2947, and 2881 cm^{-1}).

The overall intensity of the modes of the mixture of hydrocarbons and the intensities of the modes of the individual adsorbates (π-bonded ethene, di-σ-bonded ethene, ethyl, and ethylidyne) remained approximately constant during the induction period. This result indicates that buildup (if any) of hydrocarbons on the catalyst surface and/or equilibration of adsorbate concentrations occurred on a time scale much shorter than that of the induction period.

In addition to modes indicating hydrocarbon adsorbates on the clusters during the induction period for ethene hydrogenation catalysis, we observed the formation of new modes during catalysis, at 2020 and 1940 cm^{-1} (Figure 8b). The positions of these modes are similar to the values of ν_{M-H} reported for hydrogen on supported particles of platinum[52,53] and for organorhodium complexes incorporating hydrides[54,55] (Table 5). To test the inference of hydrides, we attempted an exchange experiment with D_2 immediately following ethene hydrogenation catalysis on Rh_6/La_2O_3. The expected positions of the Rh−D modes largely overlap strong absorption modes of the La_2O_3 support (1360−1510 cm^{-1}), but shoulders are evident at about 1428 and 1385 cm^{-1}, consistent with the Rh−D modes expected at about 1435 and 1378 cm^{-1} (Figure 9). Hence, the modes at 2020 and 1940 cm^{-1} in the spectra of adsorbates on Rh_6/La_2O_3 during catalysis are inferred to indicate Rh−H stretching.

Although the intensities of the hydrocarbon adsorbates remained approximately constant during the induction period, the intensities of the modes at 2020 and 1940 cm^{-1} increased from zero at the start of catalysis to their maximum values during steady-state catalysis (Figure 10).

EXAFS parameters characterizing the sample formed by decarbonylation of La_2O_3-supported hexarhodium carbonyl clusters in the presence of flowing He at 288 K (as described above) include Rh−Rh first-shell and second-shell contributions with coordination numbers of 3.8 and 1.1, respectively, at distances of 2.63 and 3.66 Å, respectively (Table 6). These results confirm the synthesis of clusters that are well approximated as Rh_6/La_2O_3, as described above.

TABLE 6: EXAFS Fit Parameters Characterizing Rh_6/La_2O_3 Scanned in Flowing He at 288 K and 760 Torr and in a Reacting Mixture of H_2 and C_2H_4 at 288 K and 760 Torr

	He (12.4 mL min^{-1})				He (150 mL min^{-1}), H_2 (75 mL min^{-1}), and C_2H_4 (75 mL min^{-1})			
backscatterer	N	R (Å)	$\Delta\sigma^2 \times 10^3$ (Å^2)	ΔE_o (eV)	N	R (Å)	$\Delta\sigma^2 \times 10^3$ (Å^2)	ΔE_o (eV)
rhodium								
1st shell	3.8	2.63	5.91	2.47	3.7	2.64	7.27	5.39
2nd shell	1.1	3.66	4.65	3.22	0.9	3.69	8.33	4.31
C ligands								
C	0.3	1.93	−5.08	0.58	0.3	1.95	−4.81	−2.03
support contributions								
O_{short}	0.9	2.08	−0.38	−3.71	0.7	2.07	−3.02	−1.87
La 1st shell	0.5	2.89	2.5	12.6	1.6	2.81	12.0	8.25
La 2nd shell	0.5	3.43	2.91	−6.21	0.3	3.39	2.19	6.64

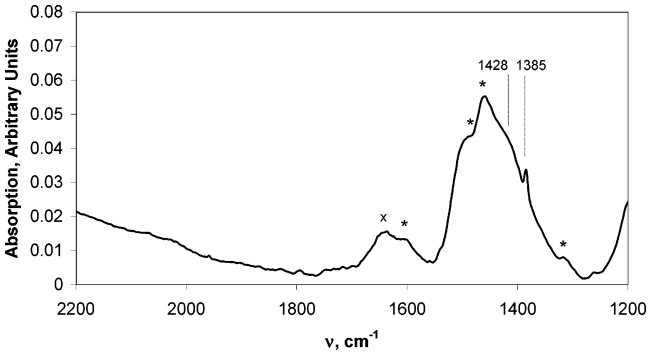

Figure 9. IR spectra of Rh_6/La_2O_3 following ethene hydrogenation at 298 K and 760 Torr with H_2 and C_2H_4, followed by purging with He (10 min at 30 mL min^{-1} NPT), then contacting with D_2. Feature marked by "X" denotes surface water. Features marked by "*" denote absorption modes of La_2O_3.

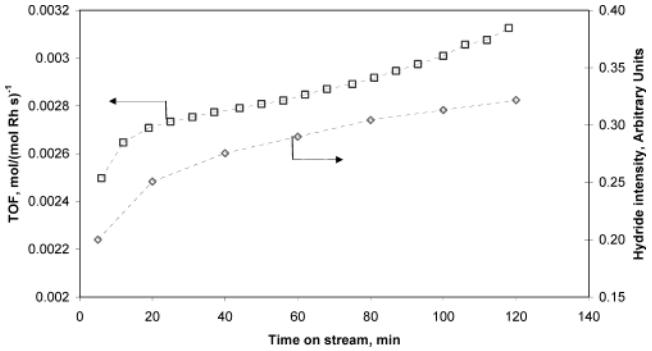

Figure 10. TOF (squares) and IR intensity of hydride (2020-cm^{-1} mode) (diamonds) during the induction period for ethene hydrogenation on Rh_6/La_2O_3 at 298 K.

EXAFS parameters characterizing the La_2O_3-supported catalyst during ethene hydrogenation catalysis at 288 K and 760 Torr (174 Torr of H_2, 156 Torr of C_2H_4, and 430 Torr of He) show that the Rh_6 cluster frame was essentially unchanged during reaction (Table 6). As the Rh_6 clusters were maintained during catalysis and the support was catalytically inactive by itself, we infer that the Rh_6 clusters were the catalytically active species.

Because the Rh−C shell was not determined with a high degree of confidence, it was not possible to ascertain additional bonding of carbonaceous species to the clusters during catalysis. Furthermore, the IR results show that the concentration of hydrocarbon adsorbates on the clusters was relatively low, consistent with the small observed EXAFS contribution.

^{1}H MAS NMR of Rh_6/La_2O_3 after Ethene Hydrogenation Catalysis. The single-pulse ^{1}H MAS NMR spectrum of Rh_6/La_2O_3 following ethene hydrogenation catalysis includes resonances at −22.8, −25.4, −26.2, and −27.3 ppm, in addition to resonances at 6.4, 5.5, and 2.0 ppm that are associated with the hydroxyl groups of the La_2O_3 support (Figure 11). The resonances observed in the range of −22 to −28 ppm are readily identified as hydrides, by comparison with the ^{1}H NMR spectra of hydrides in other materials (Table 7).[56−59]

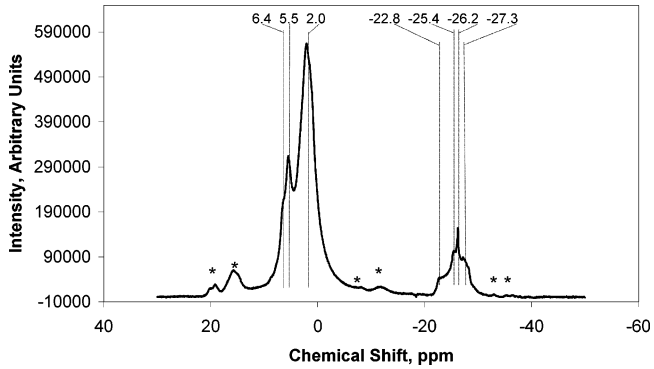

Figure 11. ^{1}H MAS NMR spectrum of La_2O_3-supported Rh_6 clusters following ethene hydrogenation catalysis at 298 K obtained at 400.1 MHz (single-pulse excitations, 5.4 kHz spinning rate, 0.1 s relaxation delay, 10 000 acquisitions). Features marked by "*" are spinning sidebands, identified by rotating the sample at 4.4 and 5.4 kHz.

TABLE 7: Summary of ^{1}H NMR Spectra: Metal Hydrides in Organometallic Complexes and on Rh_6/La_2O_3

sample	^{1}H isotropic shifts δ, ppm	ref
$[Rh_6H(CO)_{15}]^-$ in perdeuterioacetone	−12.2	58
$[Rh_6H(CO)_{15}C]^{2-}$ in perdeuterioacetone	−15.6	58
$[Rh_6H(CO)_{13}C]^{2-}$ in THF	−14.6	57
$[RhH(NH_3)_5][SO_4]$	−17.1	54
$[RhH(NH_3)(en)_2][ClO_4]_2$[a]	−16.3	55
trans-$[RhH(pn)_2(H_2O)]^{2+}$[b]	−21.7	55
hydride on Pt/Al_2O_3[c,d]	−30 (approximately)	59
hydride on Rh_6/La_2O_3	−22.8, −25.4, −26.2, −27.3[e]	this work

[a] en = ethenediamine. [b] pn = 1,2-diaminopropane. [c] Platinum particles with an average diameter of 15 Å. [d] Surface coverage of approximately 0.1. [e] Multiple resonances are attributed to inhomogeneities in the bonding of Rh_6 clusters to the La_2O_3 support, such as those associated with bonding to defects or different crystallographic planes.

Discussion

Synthesis Chemistry of Rhodium Carbonyls on Support Surface. Chini and Martinengo[60−63] demonstrated that reactions of mononuclear rhodium carbonyls give anionic rhodium carbonyl clusters in basic solutions and neutral rhodium carbonyl clusters in neutral solutions. For example, in methanol, [Rh-

$(CO)_2Cl]_2$ reacts with H_2O and CO to form neutral products, $Rh_4(CO)_{12}$ and $Rh_6(CO)_{16}$:

$$2[Rh(CO)_2Cl]_2 + 6CO + 2H_2O \rightarrow Rh_4(CO)_{12} + 2CO_2 + 4HCl \quad (1)$$

$$3[Rh(CO)_2Cl]_2 + 7CO + 3H_2O \rightarrow Rh_6(CO)_{16} + 3CO_2 + 6HCl \quad (2)$$

In more basic solutions, in the presence of Na_2CO_3, anionic rhodium carbonyl clusters such as $[Rh_6(CO)_{15}]^{2-}$ are formed:

$$6[Rh(CO)_2Cl]_2 + 7Na_2CO_3 + 2ROH \rightarrow 2Na[Rh_6(CO)_{15}(COOR)] + 4CO + CO_2 + H_2O \quad (3)$$

$$2Na[Rh_6(CO)_{15}(COOR)] + 2NaOH \rightarrow Na_2[Rh_6(CO)_{15}] + NaHCO_3 + ROH \quad (4)$$

$[Rh_6C(CO)_{15}]^{2-}$ is also formed in basic solutions, but the chemistry is not well understood. Similar chemistry of rhodium carbonyls was found to take place in the pores of the basic zeolite NaX.[5]

The results presented here show the conversion of Rh(I) dicarbonyls on La_2O_3 gives rhodium carbonyl clusters that are most likely $[Rh_6(CO)_{15}]^{2-}$ and/or $[Rh_6C(CO)_{15}]^{2-}$. The neutral $Rh_6(CO)_{16}$ is unlikely to have been formed because La_2O_3 is strongly basic.[64]

Ethene Hydrogenation Catalyzed by Rh_6/La_2O_3. Results of earlier work based on EXAFS spectroscopy of functioning catalysts indicate that supported Ir_4,[65] Ir_6,[66] and Rh_6 are catalytically active for propene hydrogenation under mild conditions. The results reported here provide additional evidence of alkene hydrogenation catalysis by supported metal clusters and add information about the role of the support and the species bonded to the clusters during catalysis.

IR spectra of the adsorbates on Rh_6/La_2O_3 measured during the induction period in the flow reactor show that the concentration of the hydrocarbon species on the catalyst was approximately constant, although the catalytic reaction rate roughly doubled. Thus, we infer that changes in the hydrocarbon adsorbates on Rh_6 were not primarily responsible for the observed increase in catalytic activity. These hydrocarbon adsorbates have been inferred to be π-bonded ethene, di-σ-bonded ethene, ethylidyne, and ethyl. As the concentrations of these adsorbates did not change substantially during the induction period, the data do not provide information about the roles of the individual hydrocarbon adsorbates in ethene hydrogenation on Rh_6/La_2O_3.

The IR data show that as the catalytic activity increased during the induction period, the intensity (and thus, we infer, the concentration) of hydride ligands on Rh_6/La_2O_3 also increased (Figure 6).[67,68] The intensity of the hydride band at 2020 cm^{-1} is correlated well with the catalytic activity (Figure 6).[69,70] Thus, the data are consistent with the inference that hydrides are reactive intermediates in ethene hydrogenation on Rh_6/La_2O_3. The data also suggest that, during catalysis, the Rh_6 clusters were nearly saturated with ethene-derived adsorbates (ethyl, ethylidyne, di-σ-bonded ethene, and π-bonded ethene), as shown by the nearly zero-order kinetics in ethene partial pressure. Thus, it is not surprising that during the induction period there was hardly any change in the composition of ethene-derived adsorbates on the clusters as the catalytic activity increased. In contrast, the relatively high reaction order in H_2 and the correlation of hydride band intensity with catalytic activity suggest that hydride concentration on the surface was limited.

TABLE 8: Catalytic Activities of Supported Metal Clusters and Extended Surfaces of Metal for Ethene Hydrogenation

catalyst	support	TOF, s^{-1}	reaction order in H_2	ref
Rh_6	La_2O_3	15.5[a,b]	1.71[d]	this work
Rh_6	MgO	0.59[a,b]	1.47[d]	11
Rh_6	γ-Al_2O_3	0.23[a,b]	1.24[d]	11
Pt(111)	none	11[c]	0.81	9

[a] Reaction conditions: 295 ± 1 K, 620 Torr of He, 100 Torr of H_2, and 40 Torr of C_2H_4. [b] Turnover frequency defined as (mol of ethane produced)(mol of Rh s)$^{-1}$. [c] Reaction conditions: 295 K, 100 Torr of H_2, and 35 Torr of C_2H_4. [d] Reaction order in H_2 determined experimentally at 273 K with a constant ethene partial pressure of 40 Torr and H_2 partial pressures ranging from 50 to 400 Torr.

The rate of ethene hydrogenation on Rh_6/La_2O_3 exhibits a stronger dependence on H_2 partial pressure (a reaction order of 1.7) than that typically observed for ethene hydrogenation on conventional platinum and nickel catalysts (reaction orders of 0.5−1.3). In catalysis by extended metal surfaces, the orders of reaction in H_2 are usually near 0.5 for low-temperature alkene hydrogenation (at temperatures of about 250 K), and as the reaction temperature increases, the reaction order in H_2 increases to 1 or even slightly higher values (1.2−1.3). A possible reason for the difference in the reaction orders in H_2 characterizing extended metal surfaces, on one hand, and supported metal clusters, on the other, might be the ease with which π-bonded ethene can be inserted into the M−H bond. A theoretical investigation suggested that the insertion of π-bonded ethene into the bond of diatomic Rh−H is a strikingly low barrier process.[71] A low barrier for insertion of π-bonded ethene into Rh−H could give rise to a strong dependence of the reaction rate on H_2 partial pressure, with Rh−H being almost immediately consumed by reaction with adsorbed ethene.

Effect of La_2O_3 Support. The effect of La_2O_3 on Rh_6 is demonstrated by a comparison of the catalytic activity of this sample for ethene hydrogenation with the activities of samples consisting of Rh_6 clusters on other supports (γ-Al_2O_3 or MgO) (Table 8). Under the same reaction conditions, Rh_6 clusters on strongly basic La_2O_3 are about 26 times more active than Rh_6 on basic MgO and 56 times more active than Rh_6 on γ-Al_2O_3. The experimentally observed reaction order in H_2 was found to be 1.7 for Rh_6 on La_2O_3, 1.5 for Rh_6 on MgO, and 1.2 for Rh_6 on γ-Al_2O_3. The various supports have different electron-donor characteristics that evidently affect the interactions of the clusters with the reactant-derived ligands. Estimates of basicities, for example by determination of the isoelectric point and the bonding of probe molecules such as acetylene, indicate that La_2O_3 and MgO are stronger bases than γ-Al_2O_3.[72−75] The acid−base properties depend on the degree of hydroxylation of the metal oxide and on the cation charges. The clusters supported on La_2O_3 and MgO are more active catalytically than those supported on the more weakly basic γ-Al_2O_3, but there is not a clear correlation of the catalytic activities or reaction orders with the base strengths reported. Further work seems to be required, such as estimates on the basis of density functional theory with account taken of the state of hydroxylation of the surface; such work is expected to be challenging because of the complexity of the surface structures and the need for simplifying assumptions in the structural models.

We suggest two possibilities: that the more basic supports promote the formation of hydride and/or increase the reactivity of adsorbed reactants, such as hydride and π-bonded ethene.

The former possibility does not account for the observations here, because an increased hydride concentration on the clusters would give rise to more nearly equilibrated hydrogen adsorption and a lower reaction order in H_2. The latter possibility, however, agrees with the data—increased electron donation from the support to the clusters could weaken the interaction of π-bonded ethene with Rh_6, increasing its reactivity, and give rise to a higher reaction order in H_2. Correspondingly, the strongly basic La_2O_3 provides the most active catalyst and the weakly basic γ-Al_2O_3 the least active.

The present observations of catalytic activities of Rh_6 are opposite those observed for supported platinum particles. Platinum particles on acidic supports have higher hydrogenation activities than metals on neutral or basic supports.[76−80] Therefore, we infer that both the composition of the metal and the cluster or particle size may play a key role in determining how the support influences the catalytic properties of a supported metal.

Conclusions

A method for forming nearly uniform, site-isolated Rh_6 clusters (with some carbon-containing ligands apparently associated with them) on La_2O_3 involves the use of He at 573 K to decarbonylate supported rhodium carbonyl clusters formed by reductive carbonylation of $Rh(CO)_2(acac)$ supported on La_2O_3. The Rh_6 clusters catalyze ethene hydrogenation at 253−297 K. EXAFS spectra show that the Rh_6 clusters retain their octahedral structure during ethene hydrogenation catalysis at 288 K, and similar results for these clusters on other supports allow a determination of support effects on the catalytic activity. IR and ^1H NMR spectroscopies used to characterize the adsorbates formed on Rh_6 during catalysis indicate hydrocarbon adsorbates (inferred to be π-bonded ethene, di-σ-bonded ethene, ethyl, and ethylidyne) and hydride. The concentration of hydrides increased during the induction, correlating well with the rate of reaction. The data are consistent with the inference that hydrides are intermediates in kinetically significant steps in the hydrogenation of ethene on Rh_6/La_2O_3. The La_2O_3 support increases the catalytic activity of Rh_6 clusters more than MgO or γ-Al_2O_3.

Acknowledgment. We thank Brian Phillips for help with the NMR spectroscopy. This research was supported by the donors of the Petroleum Research Fund, administered by the American Chemical Society. We acknowledge the Stanford Synchrotron Radiation Laboratory and the National Synchrotron Light Source for access to beam time. The EXAFS data were analyzed with the software XDAP.[23] Portions of this research were carried out at the Stanford Synchrotron Radiation Laboratory, a national user facility operated by Stanford University on behalf of the U.S. Department of Energy, Office of Basic Energy Sciences. We thank the W. M. Keck Foundation for funds to purchase the NMR spectrometer.

References and Notes

(1) Brown, K.; Tegoni, M.; Prudencio, M.; Pereira, A. S.; Besson, S.; Moura, J. J.; Moura, I.; Cambillau, C. *Nature Struct. Biol.* **2000**, *7*, 191.
(2) Miller, J. T.; Meyers, B. C.; Modica, F. S.; Lane, G. S.; Vaarkamp, M.; Koningsberger, D. C. *J. Catal.* **1993**, *143*, 395.
(3) Gates, B. C. *Chem. Rev.* **1995**, *95*, 511.
(4) Goellner, J. F.; Gates, B. C. *J. Phys. Chem. B* **2001**, *105*, 3269.
(5) Weber, W. A.; Gates, B. C. *J. Phys. Chem. B* **1997**, *101*, 10423.
(6) Weber, W. A.; Phillips, B. L.; Gates, B. C. *Chem. Eur. J.* **1999**, *5*, 2899.
(7) Argo, A. M.; Gates, B. C. *J. Phys. Chem. B* **2003**, *107*, 5519.
(8) Backman, A. L.; Masel, R. I. *J. Vac. Sci. Technol., A* **1991**, *9*, 1789.
(9) Cremer, P. S.; Su, X.; Shen, Y. R.; Somorjai, G. A. *J. Am. Chem. Soc.* **1996**, *118*, 2942.
(10) Ohtani, T.; Kubota, J.; Kondo, J. N.; Hirose, C.; Domen, K. *J. Phys. Chem. B* **1999**, *103*, 4562.
(11) Argo, A. M. Ph.D. Dissertation, University of California, 2001.
(12) Argo, A. M.; Odzak, J. F.; Lai, F. S.; Gates, B. C. *Nature* **2002**, *415*, 623.
(13) Neurock, M.; van Santen, R. A. *J. Phys. Chem. B* **2000**, *104*, 11127.
(14) Yagasaki, E.; Masel, R. I. In *Catalysis*; Spivey, J. L., Ed.; Royal Society of Chemistry: Cambridge, 1994; Vol. 11.
(15) David, C.; Seon, F. (Rhone-Poulenc Chimie, Fr.) Eur. Pat. Appl. EP, 1989.
(16) Gates, B. C.; Lamb, H. H. *J. Mol. Catal.* **1989**, *52*, 1.
(17) Jentoft, R. E.; Deutsch, S. E.; Gates, B. C. *Rev. Sci. Instrum.* **1996**, *67*, 2111.
(18) Xu, Z.; Gates, B. C. *J. Catal.* **1995**, *154*, 335.
(19) Odzak, J. F.; Argo, A. M.; Gates, B. C. *Rev. Sci. Instrum.* **2001**, *72*, 3943.
(20) Duivenvoorden, F. B. M.; Koningsberger, D. C.; Uh, Y. S.; Gates, B. C. *J. Am. Chem. Soc.* **1986**, *108*, 6254.
(21) van Zon, J. B. A. D.; Koningsberger, D. C.; van't Blik, H. F. J.; Sayers, D. E. *J. Chem. Phys.* **1985**, *82*, 5742.
(22) Kirlin, P. S.; van Zon, F. B. M.; Koningsberger, D. C.; Gates, B. C. *J. Phys. Chem.* **1990**, *94*, 8439.
(23) Vaarkamp, M.; Linders, J. C.; Koningsberger, D. C. *Physica B* **1995**, *209*, 159.
(24) Zabinsky, S. I.; Rehr, J. J.; Ankudinov, A.; Albers, R. C.; Eller, M. J. *Phys. Rev. B* **1995**, *52*, 2995.
(25) Ankudinov, A. Ph.D. Dissertation, University of Washington, 1996.
(26) *Crystal Structures*, 2nd ed.; Wycoff, R. W. G., Ed.; Wiley: New York, 1963; Vol. 1.
(27) *Crystal Structures*, 2nd ed.; Wycoff, R. W. G., Ed.; Wiley: New York, 1963; Vol. 2.
(28) van Zon, J. B. A. D. Ph.D. Dissertation, Eindhoven University of Technology, 1988.
(29) van Zon, F. B. M.; Maloney, S. D.; Gates, B. C.; Koningsberger, D. C. *J. Am. Chem. Soc.* **1993**, *115*, 10317.
(30) Coey, J. M. D. *Acta Crystallogr., Sect. B* **1970**, *B26*, 1876.
(31) Lytle, F. W.; Sayers, D. E.; Stern, E. A. *Physica B* **1989**, *158*, 701.
(32) Martinengo, S.; Chini, P. *Gazz. Chim. Ital.* **1972**, *102*, 344.
(33) Yang, A. C.; Garland, C. W. *J. Phys. Chem.* **1957**, *61*, 1504.
(34) Chini, P.; Martinengo, S. *J. Chem. Soc., Chem. Commun.* **1969**, 1092.
(35) Beck, W.; Lottes, K. *Chem. Ber.* **1961**, *94*, 2578.
(36) Vaarkamp, M. *Catal. Today* **1998**, *39*, 271.
(37) Corey, E. R.; Dahl, L. F.; Beck, W. *J. Am. Chem. Soc.* **1963**, *85*, 1202.
(38) Ciani, G.; Sironi, A.; Chini, P.; Martinengo, S. *J. Organomet. Chem.* **1981**, *213*, C37.
(39) Albano, V. G.; Sansoni, M.; Chini, P.; Martinengo, S. *J. Chem. Soc., Dalton Trans.* **1973**, 651.
(40) Goellner, J. F.; Gates, B. C.; Vayssilov, G. N.; Rösch, N. *J. Am. Chem. Soc.* **2000**, *122*, 8056.
(41) Albano, V. G.; Chini, P.; Martinengo, S.; McCaffery, D. J.; Strumolo, D.; Heaton, B. T. *J. Am. Chem. Soc.* **1974**, *96*, 8106.
(42) Goellner, J. F.; Gates, B. C. *J. Phys. Chem. B* **2001**, *105*, 3269.
(43) Cortright, R. D.; Goddard, S. A.; Rekoske, J. E.; Dumesic, J. A. *J. Catal.* **1991**, *127*, 342.
(44) Shimanouchi, T. *Tables of Molecular Vibrational Frequencies*; National Bureau of Standards: Washington, DC, 1962.
(45) Bent, B. E.; Mate, C. M.; Kao, C.-T.; Slavin, A. J.; Somorjai, G. A. *J. Phys. Chem.* **1988**, *92*, 4720.
(46) Beebe, J.; T. P.; Yates, J.; J. T. *J. Phys. Chem.* **1987**, *91*, 254.
(47) Bol, C. W. J.; Friend, C. M. *J. Phys. Chem.* **1995**, *99*, 11930.
(48) Keol, B. E.; Bent, B. E.; Somorjai, G. A. *J. Chem. Phys.* **1984**, *146*, 211.
(49) Steininger, H.; Ibach, H.; Lehwald, S. *Surf. Sci.* **1982**, *117*, 685.
(50) Lloyd, K. G.; Roop, B.; Campion, A.; White, J. M. *Surf. Sci.* **1989**, *214*, 227.
(51) Merrill, P. B.; Madix, R. J. *J. Am. Chem. Soc.* **1996**, *118*, 5062.
(52) Shahid, G.; Sheppard, N. *Spectrochim. Acta, Part A* **1990**, *46A*, 999.
(53) Soma, Y. *J. Catal.* **1982**, *75*, 267.
(54) Thomas, K.; Osborn, J. A.; Powell, A. R.; Wilkinson, G. *J. Chem. Soc. A* **1968**, 1801.
(55) Thomas, K.; Wilkinson, G. *J. Chem. Soc. A* **1970**, *1970*, 356.
(56) Crabtree, R. H. *The Organometallic Chemistry of the Transition Metals*, 2nd ed.; Wiley: New York, 1994.
(57) Bordoni, S.; Heaton, B. T.; Seregni, C.; Strona, L.; Goodfellow, R. J.; Hursthous, M. B.; Thornton-Pett, M.; Martinengo, S. *J. Chem. Soc., Dalton Trans.* **1988**, 2103.
(58) Heaton, B. T.; Strona, L.; Martinengo, S.; Strumolo, D.; Goodfellow, R. J.; Sadler, I. H. *J. Chem. Soc., Dalton Trans.* **1982**, 1499.

(59) De Menorval, L. C.; Fraissard, J. P. *Chem. Phys. Lett.* **1981**, *77*, 309.
(60) Chini, P.; Martinengo, S. *Inorg. Chim. Acta* **1969**, *3*, 21.
(61) Chini, P.; Martinengo, S. *Inorg. Chim. Acta* **1969**, *3*, 299.
(62) Chini, P.; Martinengo, S. *Inorg. Chim. Acta* **1969**, *3*, 315.
(63) Chini, P.; Martinengo, G.; Giordano, G. *Gazz. Chim. Ital.* **1972**, *102*, 330.
(64) Triantafillou, N. D.; Gates, B. C. *Langmuir* **1999**, *15*, 2595.
(65) Panjabi, G.; Argo, A. M.; Gates, B. C. *Chem. Eur. J.* **1999**, *5*, 2417.
(66) Weber, W. A. Ph.D. Dissertation, University of California, 1997.
(67) Satterfield, C. N. *Mass Transfer in Heterogeneous Catalysis*; M.I.T. Press: London, 1970.
(68) Weisz, P. B.; Hicks, J. S. *Chem. Eng. Sci.* **1962**, *17*, 265.
(69) Goddard, S. A.; Cortright, R. D.; Dumesic, J. A. *J. Catal.* **1992**, *137*, 186.
(70) Rekoske, J. E.; Cortright, R. S.; Goddard, S. A.; Sharma, S. B.; Dumesic, J. A. *J. Phys. Chem.* **1992**, *96*, 1880.
(71) Siegbahn, P. E. M. *J. Am. Chem. Soc.* **1993**, *115*, 5803.
(72) Brunelle, J. P. *Stud. Surf. Sci. Catal.* **1979**, *3*, 211.
(73) Knözinger, H.; Huber, S. *J. Chem. Soc., Faraday Trans.* **1998**, *94*, 2047.
(74) Lavalley, J. C. *Catal. Today* **1996**, *27*, 377.
(75) Ivanov, A. V.; Koklin, A. E.; Uvarova, E. B.; Kustov, L. M. *Phys. Chem. Chem. Phys.* **2003**, *5*, 4718.
(76) Miller, J. T.; Modica, F. S.; Meyers, B. L.; Koningsberger, D. C. *Prepr. Pap.—Am. Chem. Soc., Div. Pet. Chem.* **1993**, *38*, 825.
(77) Larsen, G.; Haller, G. L. *Catal. Lett.* **1989**, *3*, 103.
(78) Karpinski, Z.; Gandhi, S. N.; Sachtler, W. M. H. *J. Catal.* **1993**, *141*, 337.
(79) Mojet, B. L.; Kappers, M. J.; Muijsers, J. C.; Niemantsverdriet, J. W.; Miller, J. T.; Modica, F. S.; Koningsberger, D. C. *Stud. Surf. Sci. Catal.* **1994**, *84*, 909.
(80) Mojet, B. L.; Kappers, M. J.; Miller, J. T.; Koningsberger, D. C. *Stud. Surf. Sci. Catal.* **1996**, *101*, 1165.